JOURNAL OF GEOPHYSICAL RESEARCH, VOL. 108, NO. B2, 2132, doi:10.1029/2001JB000569, 2003

Earth tide and tilt detection by a ring laser gyroscope

K. Ulrich Schreiber and Thomas Klügel
Forschungseinrichtung Satellitengeodäsie, Technische Universität München, Kötzting, Germany

Geoffrey E. Stedman
Department of Physics and Astronomy, University of Canterbury, Christchurch, New Zealand

Received 17 April 2002; revised 21 October 2002; accepted 13 December 2002; published 28 February 2003.

[1] An Earth tide signal at the lunar tidal period of 12 hours 25 min has been detected in the Sagnac frequency record of the C-II ring laser 30 m underground at Christchurch, New Zealand. Its amplitude, one part per million of the Earth rotation signal, is much greater than the value of 40 parts per billion expected. Tiltmeter records show that a substantial part of this amplification is geophysical, the lunar component of tilt having an amplitude of the order of 0.1–0.2 μrad, principally because of ocean loading of Banks Peninsula. The joint records also show effects on the Sagnac frequency associated with cavern deformation under ambient pressure and temperature change and with long-period waves in cavern tilt. *INDEX TERMS:* 0649 Electromagnetics: Optics; 0994 Exploration Geophysics: Instruments and techniques; 1239 Geodesy and Gravity: Rotational variations; 1249 Geodesy and Gravity: Tides—Earth; 1255 Geodesy and Gravity: Tides—ocean (4560); *KEYWORDS:* ring laser, Sagnac effect, earth tides, gyroscope, ocean loading

Citation: Schreiber, K. U., T. Klügel, and G. E. Stedman, Earth tide and tilt detection by a ring laser gyroscope, *J. Geophys. Res.*, *108*(B2), 2132, doi:10.1029/2001JB000569, 2003.

1. Introduction

[2] Large ring interferometers are susceptible to solid Earth tides. This was first found accidentally in the electron-positron storage ring low-energy protons (LEP) [*Arnaudon et al.*, 1995]. *Rautenberg et al.* [1997] predicted that a lunar signal should be visible in a ring laser gyroscope such as the C-II instrument, a well-engineered square ring with side 1 meter, in the bunker 30 m underground at Cashmere, Christchurch, New Zealand. We report here the successful detection of this lunar signal and set the discussion in the wider context of an analysis of tilt effects in the Cashmere cavern. In both these cases, identification of the mechanism for coupling the lunar tidal deformations has some curious twists. While confirming some predictions, the experimental results we report have also added new puzzles.

[3] In the case of LEP the coupling mechanism was through nonhydrostatic tidal strain, or deformation of the shape of the ring. This effect, of the order of tens of parts per billion, altered the orbit of the circulating particles relative to the guiding devices commensurately; its effects were then amplified by a factor of order 1000 to the point of visibility because of the relatively large effect of such beam walk on the beam line particle energy, via the corrective steering action of the guiding quadrupole magnets.

[4] *Rautenberg et al.* [1997] considered two possible coupling mechanisms for Earth tides in a ring laser. Again, both terms were estimated to be typically $\sim 4-8 \times 10^{-8}$ of Earth rotation. However, neither of these was above the strain field. The 600-kg 1.2-m square Zerodur monolith in which the laser beam path was engineered is separated from a granite base by three small Teflon pads at the corners of a triangle of side 50 cm, and this was believed to isolate the monolith from strain in the solid Earth. Strains arising from the gravity gradient ($\sim 2 \times 10^{-13}$ Hz^2) from the direct action of the Moon are far lower, of the order of 10^{-21}.

[5] The first mechanism considered was the obvious gyroscopic effect traditional to such devices, in which the induced vorticity, or the rotational part (curl) of the Earth's deformation field, was to be monitored. Within the standard model used for the elastic properties of the Earth (notably the assumption that the elastic moduli are functions of depth but not latitude or longitude), this term vanished for a horizontal ring such as C-II.

[6] The second mechanism considered was tilt; the Sagnac beat frequency δf of the counterrotating beams in a ring laser is dependent not only on the magnitude of the local rotation $\boldsymbol{\Omega}$ relative to the local Lorentz frame but also on the angle of projection of that rotation vector on the area vector $\mathbf{A}$ of the ring, through the standard ring laser equation [*Stedman*, 1997]

$$\delta f = \frac{4A}{\lambda P}\mathbf{n} \cdot \Omega, \tag{1}$$

where λ is the wavelength of the laser and P is the perimeter. However, terms at typically tens of parts per billion of Earth rotation were well beyond the capabilities of C-II at that time (1997).

[7] In the intervening years, several major improvements have been made to C-II. Following a method standard for ring laser gyroscopes, the original strategy was to stabilize the perimeter of C-II (and hence its optical frequency, itself

0148-0227/03/2001JB000569$09.00

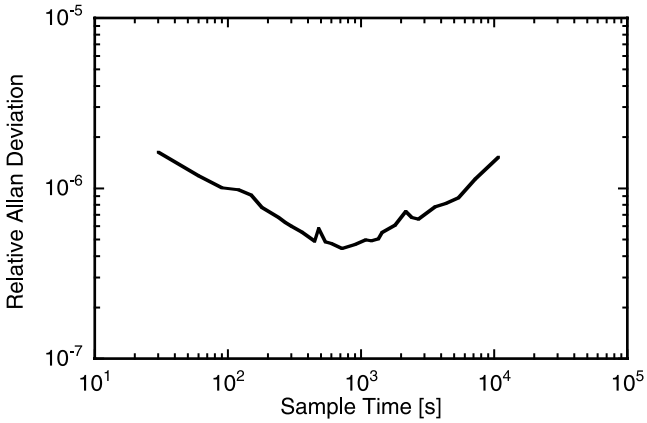

Figure 1. Plot of the relative Allan deviation of the C-II ring laser obtained from Sagnac frequency measurements taken at the end of the year 2000.

monitored against an iodine-stabilized He-Ne laser) by servoing the position of one mirror which was mounted on a relatively flexible support (May–December 1997). Although this indeed achieved Sagnac frequency stabilization by a factor of 10 over the free-running ring, residual drifts were still strong and were heavily dependent on ambient pressure and temperature fluctuations. This was eventually understood as reflecting the amplification of backscatter effects in the ring, because the induced frequency pulling was interferometrically dependent on the separation of each pair of mirrors which cause backscatter; overall perimeter stabilization through the motion of one mirror was not an effective way of stabilizing all these distances. Perimeter stabilization was then abandoned and the optical geometry and mirror mounting were fully symmetrized (in December 1998). It was expected that with a free-floating but symmetrical ring, the relative phase of backscattered beams would remain constant to first order under pressure and temperature variations since (apart from mode jumps) the optical wavelength would scale in proportion to all the mirror separations [*Schreiber et al.*, 1998]. Indeed a dramatic reduction in drift was obtained [*Schreiber et al.*, 1999]. More recently again (December 1999), C-II was placed inside a pressure vessel stabilized in pressure to ±0.1 hPa, to further reduce the residual direct effects of ambient pressure variations. With this level of environmental isolation, C-II has produced Allan deviations below the parts per million level with sampling times of order 1000 s; we report here one example (Figure 1) in which a relative Sagnac frequency stabilization of less than 5×10^{-7} was obtained.

2. Orientation of a Large Ring Laser

[8] The local tilts were measured using an Applied Geomechanics model 701 tiltmeter, placed on top of the ring laser inside the pressure vessel. The recorded peak-to-peak amplitudes of the semidiurnal tidal waves are in the range of 0.2–0.4 μrad. The tidal signal is assumed to be strongly affected by the nearby ocean. Thus a computation of the body tides as well as the ocean loading tides was performed using routines of the SPOTL-package [*Agnew*, 1997]. The body tide program (ertid) assumes an elastic Earth with Love numbers $h_2 = 0.6114$, $k_2 = 0.304$, and $l_2 = 0.0832$. The accuracy of 10^{-3} relative to a very complete ephemeris is sufficient for our purpose. The computation of the ocean loading tides include three steps. First, the main tidal harmonic constants were computed with nloadf for the location of C-II (172.623°E, 43.575°S) using different ocean tide models (FES 95.2, CSR 3.0, and TPXO.2) and Green functions for a Gutenberg-Bullen A average Earth. In a second step the results were extracted from the tidal load file using harprp, and finally a time series of tidal tilts was computed from the harmonic constants using hartid.

[9] The time series of the ocean tide models coincide in phase but differ in amplitude by up to 15%. The model FES 95.2 shows the best fit because of its largest amplitudes. The resulting time series of body and ocean loading tides were then multiplied by a varying factor and subtracted from the observed tilts until the tidal waves disappeared. The phase lag between the body and the ocean loading tides allows a clear separation between both components. In the north-south direction the resulting factor for the ocean loading tides was 0.98 indicating a very good agreement with the ocean load model. The tidal waves in the residual time series can only be explained if tilt-strain coupling is taken into account. Tilt-strain coupling occurs when (homogenous) strain fields are distorted in the vicinity of inhomogeneities like cavities, producing anomalous tilts (cavity effect). These tilts can reach significant magnitudes near corners, ledges, or cracks [*Harrison*, 1976]. Since the ring laser is located near the south wall of the cave, this mechanism is likely to influence tidal tilt measurements. Using the time series for body tide strain in north direction and applying a factor of 2.4 nanorad/nanostrain, the residual tidal waves could almost completely be removed. Figure 2 shows a time series of the measured tilt, the computed tilt and the residual tilt over an arbitrarily chosen period of 20 days.

[10] A similar procedure for the east-west direction yields a factor for the ocean loading tides of 1.04 and a tilt-strain coupling factor of −1.3 nrad/nstrain. In the residual time series there is still a tidal signal that cannot be removed in this way. However our ring laser is not sensitive to small east-west orientation changes. Therefore we have not investigated this issue further.

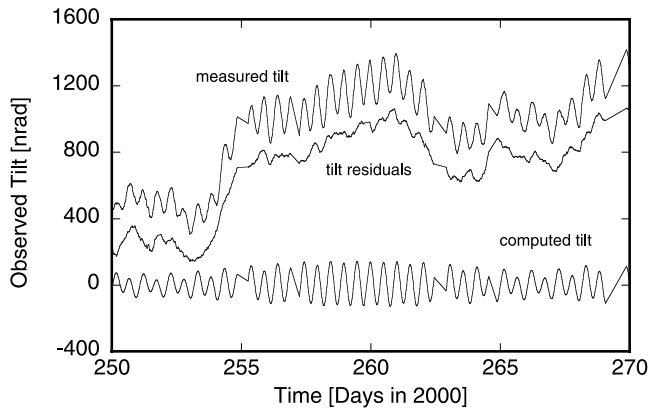

Figure 2. Time series of the measured tilt, the computed theoretical tilt, and the residual tilt which remains after subtracting the theortically computed tides from the observation. (Discontinuities in the time series are coming from gaps in the observations.)

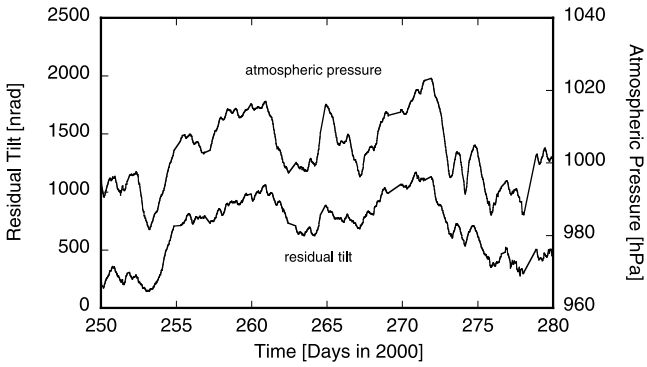

Figure 3. Comparison of the residual north-south tilt as observed at the ring laser with the local atmospheric pressure. The high correlation may be coming from deformations of the cave (cavity effect) or regional crustal deformations as the result of the inverse barometer effect.

[11] Both residual time series show a high correlation with the local atmospheric pressure, as Figure 3 shows. A linear regression results in a gradient of 21.6 nrad/hPa with a correlation coefficient of 0.87 for the north-south direction and a gradient of −8.2 nrad/hPa with a correlation coefficient of 0.56 for the east direction, resulting in a tilt toward NNW when the atmospheric pressure increases. This effect can either be due to a local cavity effect according to the mechanism described above (see also section 4), or a regional deformation of the crust, which may reach this order of magnitude near coastlines due to the inverted barometer effect of the ocean [*Rabbel and Zschau*, 1985]. However, it is not of importance to a ring laser whether the orientation changes come from local or regional deformations, since it responds to all the tilt that is experienced directly at the instrument.

[12] It has been shown that the measured tidal tilts in the Cashmere cave are mainly crustal deformations due to ocean loading and to a lesser extend body tides. The tiltmeters are affected by crustal or local deformations as well as deflections of the vertical by attractional forces, while the ring laser only feels deformational tilts. In order to compare the effect of orientation changes obtained from the ring laser one has to remove the attractional component of the body tides according to

$$\tau_{\mathrm{def}} = \tau_{\mathrm{obs}} - \tau_{\mathrm{attr}} = \tau_{\mathrm{obs}} - \tau_{\mathrm{bt}}/(1 + k2 - h_2) \approx \tau_{\mathrm{obs}} - \tau_{bt}/0.693, \quad (2)$$

where τ_{def}, τ_{attr}, τ_{obs}, and τ_{bt} are the deformational, attractional, observed, and body tidal tilts, respectively.

3. Earth Tides in Ring Laser Data

[13] Various error sources are causing a slow drift in ring laser measurements of Earth rotation, some of which are instrumental while others are environmental. Instrumental drift sources are coming from scaling factor variations, null-shift and beam coupling from backscattering [*Aronowitz*, 1971]. Environmental drift sources are either acting as modifications to the boundary conditions of the instrumental error sources or cause independent contributions, for example by orientation changes due to cavern deformations (Figure 3). All these error sources have in common that they usually change the measured Sagnac frequency very slowly, i.e., with periods much longer than a day. Well-known strictly periodic semidiurnal orientation variations of our ring laser therefore are of great interest to evaluate the instrumental sensitivity. We will show that a careful distinction between direct and indirect ring laser responses must be drawn.

3.1. Indirect Ring Laser Response

[14] The C-II ring laser has been recording continuously over most of the calender years of 1999–2000. Since a pressure stabilizing vessel was put around the ring laser at the end of 1999 this allows an investigation of the ring laser drift with and without ambient pressure stabilization. In the following we are reporting on both operating conditions. A substantial drift upward in the Sagnac frequency is evident in the data beginning in January 1999, which is progressively slowing down until March. It is believed that this was due to the cooling of the ring laser body after the mirror upgrade in December 1998. So this part of the time series was not used in the following. Another data set, taken between day 150 and day 190 in 1999 (Figure 4, curve a) was used for the following analysis instead.

[15] Each ring laser data set contains simultaneous measurements of the epoch, the Sagnac frequency, the ring laser temperature, and the atmospheric pressure at half hour intervals. Since the time interval between measurements of the Sagnac frequency and the environmental parameters is not always exactly equidistant, an interpolator was used to generate an input data set for the power spectrum calculation. A known artificially generated sample data set was used to ensure that there are no artifacts introduced by the interpolator or the spectral analysis. In the next step the time series of the atmospheric pressure record of the ring laser data set was analyzed, as well as the effective length of the laser cavity and the Sagnac frequency. We have observed the free spectral range (FSR) of $c/P \approx 75$ MHz (c is the vacuum velocity of light, $P = 4$ m is the perimeter of the C-II ring laser) as a function of time, which is one way of monitoring the mechanical stability of a ring laser cavity. Figure 5 shows the obtained spectra for atmospheric pressure, the FSR, and the Sagnac frequency.

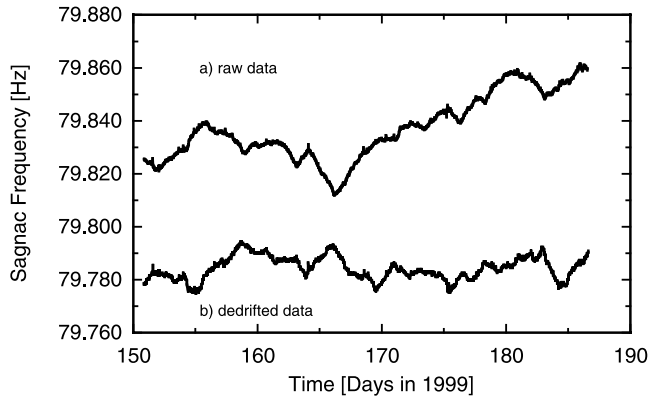

Figure 4. Time series of the Sagnac frequency (curve a) as obtained in the middle of 1999. Curve b represents the same data set after the application of a simple correction model. This data set is offset by −50 mHz for a better presentation.

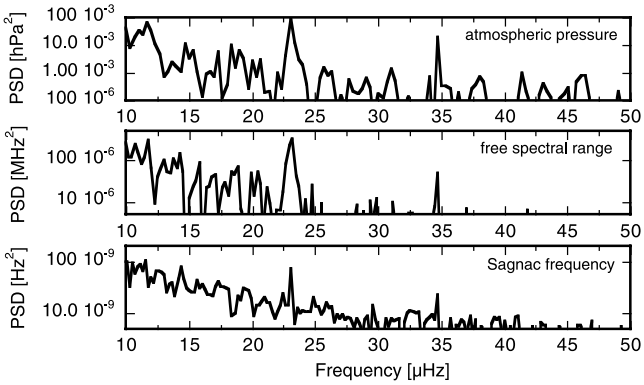

Figure 5. Power spectrum of the atmospheric pressure, the free spectral range (FSR), and the Sagnac frequency, measured with the C-II ring laser in the Cashmere Cavern at Christchurch, New Zealand. All three measurement quantities show weak but distinct frequency components of 23.2 and 34.7 μHz corresponding to periods of 12 and 8 hours, respectively.

[16] Two spectral components with a period of 12 and 8 hours are clearly present in all data sets. They are caused by global atmospheric tides [*Kertz*, 1969]. A third frequency at an inverse of 24 hours is barely visible in the noise and therefore neglected. Also other far smaller components are not considered here, nor anything with a period longer than a day. The typical overall variation of atmospheric pressure has a peak to peak value of ~40 hPa in Christchurch. The amplitude for the best visible atmospheric tides signal with a 12-hour period corresponds to 0.13 hPa. Since the ring laser was exposed to these variations in the atmospheric pressure, it was expected that the small periodic 12-hour pressure modulation could be extracted from the spectrum of the time series of the raw Sagnac frequency in the presence of much larger aperiodic changes. Given that we have a periodic expansion and compression of the C-II ring laser body by the atmospheric tides, these geometrical changes also show up in the power spectrum of the time series of the FSR. Since the amplitude of these periodic cavity length variations of 4 nm is so small, variations of the scaling factor $(4A)/(\lambda P)$ can be excluded as a cause. Frequency pulling by backscatter phase variations [*Schreiber et al.*, 1998], however, may well generate such a response of periodic Sagnac frequency variations.

3.2. Direct Ring Laser Response

[17] Under normal operating conditions, there is a substantial sensitivity of the C-II ring laser to variations in the ambient temperature and the local atmospheric pressure. The deviations of the measured Sagnac frequency are highly correlated to these environmental changes. Because of the stable monolithic construction of the ring laser body the correlation factor changes very slowly. So the measured temperature of the ring body as well as the atmospheric pressure were used as a function of time to derive a correction for the time series of the Sagnac frequency. While the original data set is shown in Figure 4, curve a, an improved data set was obtained after the corrections were applied. An additional constant value of −50 mHz offsets Figure 4, curve b, for better viewing. This corrected data set was subjected to the same spectral analysis as the original data set. As expected, the noise level coming from the ring laser drift reduced substantially, as well as the contribution from the modulation of the atmospheric tides to the spectrum. Because of this Earth tides with the period of half a lunar day (M_2) are starting to become visible in the noise. Figure 6 (top) shows the corresponding spectrum.

[18] At the end of the year 1999 a pressure stabilizing vessel was installed around the C-II ring laser in order to stabilize the scaling factor by keeping atmospheric pressure variations away from the instrument. The pressure inside the vessel is actively controlled to within ±0.1 hPa in the expectation that a spectral analysis of another long data set would give a much cleaner spectrum of lunar tides (Figure 6, bottom). There is clear evidence of the Earth tides at a frequency of 22.304 μHz that agrees to within 70 nHz with the theoretical value of 22.371 μHz. This is clearly within the spectral resolution of ±196 nHz of the time series. The corresponding frequency established from a time series of north-south tilts of the tiltmeter on top of the ring laser inside the pressure vessel has a value of 22.369 μHz, which also agrees well.

[19] In order to compare the measured time series of the ring laser Sagnac frequency to the theoretically computed time series of body tides and ocean loading we have band-pass-filtered the noisy ring laser output of the pressure stabilized data set from the year 2000, using an 8th degree Butterworth filter with a lower cutoff frequency of 15 μHz and a higher cutoff frequency of 50 μHz, respectively. The theoretical tidal tilts then were expressed as a contribution to the Sagnac frequency using the scaling factor of the C-II ring laser for the conversion. To our surprise, we had to scale this geophysical signal by a factor of 10 in order to roughly match the amplitude of the actually measured Sagnac signal variation as displayed in Figure 7. Considering the very low signal-to-noise ratio we have obtained a reasonably good agreement between the two signals in the comparison.

[20] This result impressively shows the high sensitivity of the C-II ring laser to both small ambient parameter changes and geophysical signals. The strictly periodic nature of the

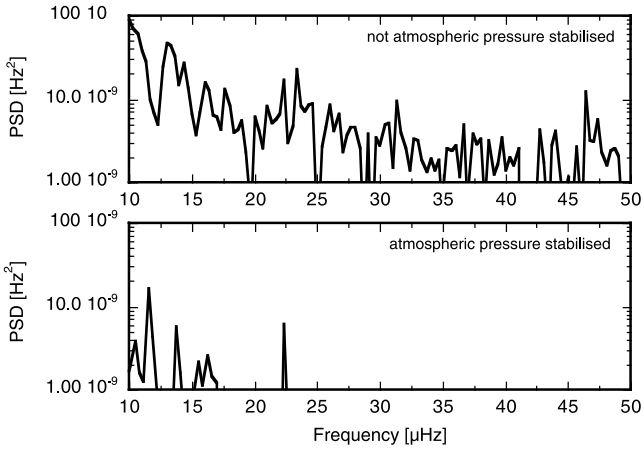

Figure 6. Spectrum of the Sagnac frequency (top) of the corrected data set of Figure 4, curve b. The lunar tide signal with a period of 12.42 hours (22.37 μHz) is just becoming visible. (bottom) Spectrum of an pressure stabilized data set taken in the year 2000.

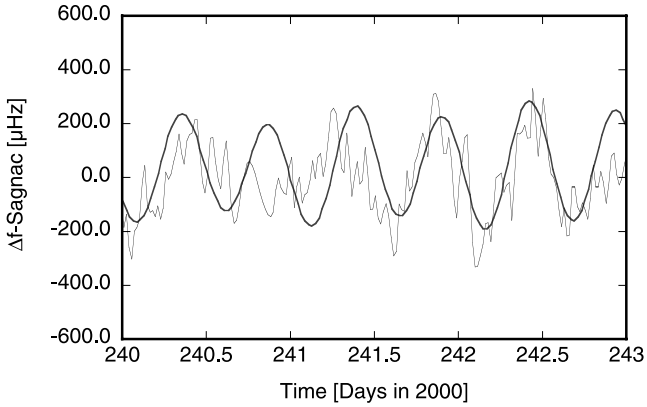

Figure 7. Comparison of a band-pass-filtered time series of the C-II ring laser output to the theoretically computed tidal tilts (body tides and ocean loading) at the ring laser site in Christchurch. The tides signal was converted to a Sagnac frequency and multiplied by 10 in order to match the amplitude of the ring laser output signal variation.

tidal effects made their identification at the resolution limit of the C-II ring laser possible. Unexpectedly we have seen a roughly tenfold increased sensitivity of C-II to signal variations whose nature is not covered by the existing ring laser perturbation theory. We currently believe that this mechanism is also responsible for the extremely high sensitivity of the instrument to changes in atmospheric pressure and ambient temperature, which are far too small to be explained by variations of the instrumental scaling factor. The perimeter stays constant at the nanometer level as the measurement series of the FSR shows. Furthermore, there are considerable indications that the cave itself is subject to aperiodic deformations which affect the orientation of the ring laser body and at a higher scale of resolution causes a systematic bias to the Sagnac frequency.

4. Cave Deformations

[21] As a result of a comparison of atmospheric pressure measured at the Christchurch airport ~20 km away and

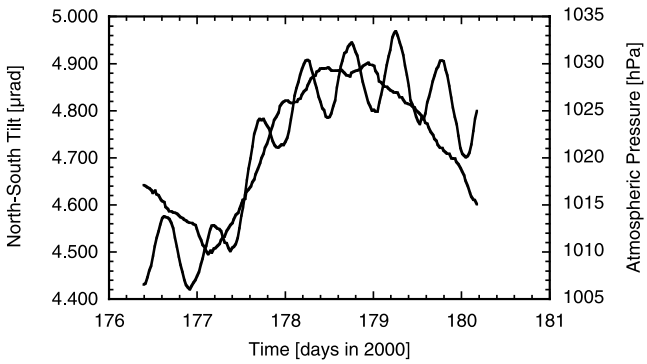

Figure 8. Deformation of the Cashmere cave as a consequence of atmospheric pressure gradients between inside and outside the cave. The periodically modulated curve was obtained from the tiltmeter (left scale), while the air pressure was measured inside the cave (right scale).

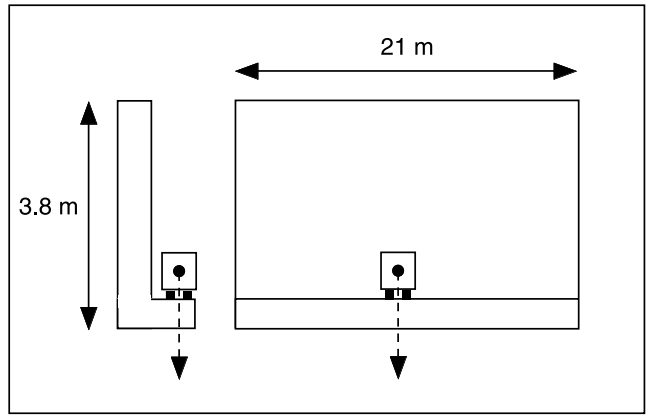

Figure 9. Outline of the location of a local-gravity-sensing tiltmeter placed on a lower ledge of a concrete wall at the back of the Cashmere Cave.

inside the cave, we found good agreement for periods of stable atmospheric conditions. For periods of rapid or large atmospheric pressure changes we obtained gradients of up to 10 hPa. The cave has only very limited ventilation in order to ensure stable temperature conditions. Therefore the signature of the atmospheric pressure changes appears low-pass-filtered inside the cave. In a very much simplified layout of the cave, there is an approximate area for the ceiling of 540 square meters and ~150 m^2 for the northern sidewall. As the cave sits in the northern slope of Banks Peninsula, let us assume that only the ceiling and the northern sidewall are subjected to the pressure difference. This means the rocks of the cave have to balance a force which is roughly corresponding to a load of 7 t per hPa pressure difference. Since the cave was blasted out of a volcano structure which consists of layers of soft material on top of layers of hard lava, it is plausible that such pressure gradients are deforming the cave. Small cracks in the rock as a result of the blasting may considerably weaken the cavity structure in addition. Figure 8 gives an example. It shows an overlay of roughly 4 days of tilt measurement and the atmospheric pressure measured inside the cave between 24 and 28 June 2000. A difference of >20 hPa

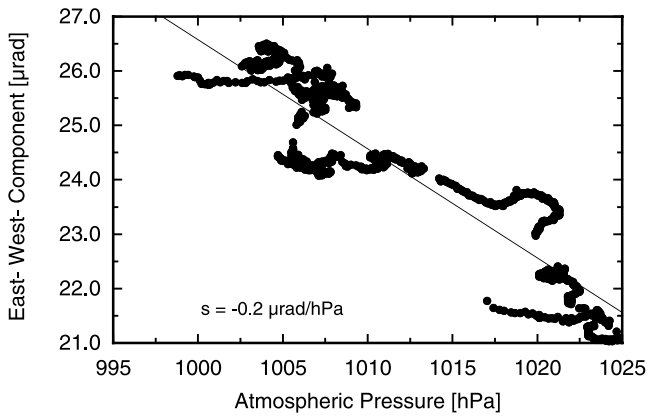

Figure 10. Observed tilts of the west wall at the back of the cave as a function of atmospheric pressure. As the pressure goes down the wall is leaning into the cave (east-west direction) with 0.2 μrad/hPa.

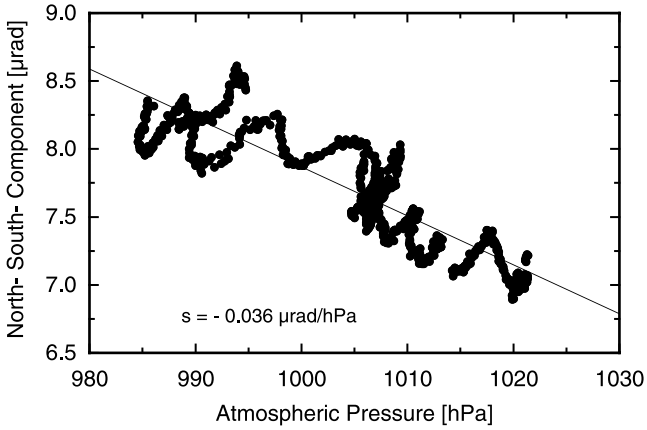

Figure 11. Observed tilts of the west wall at the back of the cave as a function of atmospheric pressure. The observed tilts along the wall (north-south direction) are much smaller.

was obtained in about a day. Apart from the periodic tilts at the lunar cycle we also notice a pressure induced change of orientation of the ring laser monument as a result of an experienced pressure change. This adds orientation related noise to the Sagnac frequency of the ring laser.

[22] In order to understand the response of the cave to atmospheric pressure changes, measurements have been carried out at a concrete wall at the back of the Cashmere cavern. Our tiltmeter was placed on a lower ledge of a reinforced concrete wall which is approximately 3.8 m high and 21 m wide. Figure 9 outlines the experimental setup.

[23] Continuous registrations of the tilts with respect to the local **g** vector were carried out over 2 weeks along with the atmospheric pressure and the temperature at the sensor. Looking at the time series of the tilt measurements of the west wall one finds the same amplitudes of the Earth tides as on the ring laser monument. In addition to that there is also a pattern of tilt from another source. However, if the tilt measurements are displayed as a function of the atmospheric pressure taken inside the cave, one can obtain the deformation or tilt of the concrete wall as a response to the atmospheric loading. Figures 10 and 11 show this behavior.

[24] Comparing the measurements of the two horizontal components (Figures 10 and 11), one can see that the wall is leaning back as the pressure goes up. As the pressure goes down the wall is tilting farther into the cave. We obtained for a measurement series of reasonably stable temperature a value of 0.2 µrad/hPa for pressure-induced wall tilt. The movements along the wall in the north-south direction to which our gyroscope is sensitive are much smaller namely 0.036 µrad/hPa.

5. Conclusion

[25] Even though the monument of the ring laser was carefully attached to the rocks of the Banks Peninsula inside a cave 30 m underground there are still clearly measurable influences on the orientation of the gyroscope from lunar tidal effects and atmospheric loading on the solid Earth. The separate tilt measurements demonstrate that the unexpectedly strong tidal signal reflects mostly the effect of ocean loading near the location of the experiment. However, the tidal effect must also involve a further amplification mechanism whose origin is presently obscure and requires further study. As the sensitivity improves, for example, with the larger ring lasers now under construction in Germany (G [*Stedman*, 1997]) and at Cashmere (UG1 [*Dunn et al.*, 2002]), we expect to see other effects from atmospheric pressure fluctuations at a lower level. Using the known periodic tidal tilts as an distinct geophysical excitation of the ring laser helped to distinguish between the sensor response and laser beam perturbation. At this stage we are still neglecting effects from polar motion, but eventually, these also may be expected to become detectable.

[26] **Acknowledgments.** These C-II ring laser results were possible because of a collaboration of Forschungseinrichtung Satellitengeodäsie of the Technische Universität München, Germany; University of Canterbury, Christchurch, New Zealand; and Bundesamt für Kartographie und Geodäsie, Frankfurt, Germany. University of Canterbury research grants U6272, U6338, also contracts UOC 503 and 802 of the Marsden Fund of the Royal Society of New Zealand are gratefully acknowledged. U. Schreiber and T. Klügel are grateful for the support from DFG on grant SCHR641/1.

References

Agnew, D. C., NLOADF: A program for computing ocean-tide loading, *J. Geophys. Res.*, *102*, 5109–5110, 1997.

Arnaudon, L., et al., Effects of terrestrial tides on the LEP beam energy, *Nucl. Instrum. Methods Phys. Res., Sect. A*, *357*, 249–252, 1995.

Aronowitz, F., The laser gyro, in *Laser Applications*, vol. 1, edited by M. Ross, pp. 133–200, Academic, New York, 1971.

Dunn, R. W., D. E. Shabalin, R. J. Thirkettle, J. G. MacDonald, G. E. Stedman, and K. U. Schreiber, Design and initial operation of a 367 m^2 rectangular ring laser, *Appl. Opt.*, *41*, 1685–1688, 2002.

Harrison, J. C., Cavity topographic effects in tilt and strain measurements, *J. Geophys. Res.*, *81*, 319–328, 1976.

Kertz, W., *Einführung in die Geophysik I, BI Hochschultaschenbücher*, 275, Springer-Verlag, New York, 1969.

Rabbel, W., and J. Zschau, Static deformations and gravity changes at the earth's surface due to atmospheric loading, *J. Geophys.*, *56*, 81–99, 1985.

Rautenberg, V., H.-P. Plag, M. Burns, G. E. Stedman, and H.-U. Jüttner, Tidally induced Sagnac signal in a ring laser, *Geophys. Res. Lett.*, *24*, 893–896, 1997.

Schreiber, U. K., C. H. Rowe, D. N. Wright, S. J. Cooper, and G. E. Stedman, Precision stabilization of the optical frequency in a large ring laser gyroscope, *Appl. Opt.*, *37*, 8371–8381, 1998.

Schreiber, U., M. Schneider, C. H. Rowe, G. E. Stedman, and W. Schlüter, Stabilising the operation of a large ring laser, in *Proceedings of the Symposium Gyro Technology 1999*, edited by H. Sorg, pp. 14.0–14.7, Univ. Stuttgart, Inst. A für Mech., Stuttgart, Germany, 1999.

Stedman, G. E., Ring laser tests of fundamental physics and geophysics, *Rep. Prog. Phys.*, *60*, 615–688, 1997.

T. Klügel and K. U. Schreiber, Technische Universität München, Forschungseinrichtung Satellitengeodäsie Fundamentalstation Wettzell, D-93444 Kötzting, Germany. (kluegel@wettzell.ifag.de; schreiber@wettzell.ifag.de)

G. E. Stedman, Department of Physics and Astronomy, University of Canterbury, Private Bag 4800, Christchurch, New Zealand. (g.stedman@phys.canterbury.ac.nz)